10^{-7} S m^2 J^{-1} for H$_2$P and ZnP respectively at room temperature. The presence of the central zinc atom therefore seems to increase the conductive properties of the solid slightly.

In Fig. 2, $(\Delta\sigma/D)_0$ is plotted as a function of temperature. For H$_2$P, a single, sharp decrease occurs at the transition from the solid to the isotropic liquid. No conductivity could be detected in the isotropic phase. For ZnP, the conductivity decreases abruptly, but does not disappear completely, at the solid to liquid-crystal transition temperature. The conductivity in the mesophase is a factor of ~3 less than in the solid with $(\Delta\sigma/D)_0 = 0.5 \times 10^{-7}$ S m^2 J^{-1}. This increases slightly with further increase in temperature in the mesophase and then suddenly drops to zero at the clearing point of ZnP.

We conclude that the long-range columnar order of porphyrin moieties in the solid and liquid-crystalline phases is essential for the conductive properties observed. In the isotropic liquid phase, any molecular organization that might occur must be of such a limited temporal or geometrical extent that it cannot support charge conduction. The results provide definitive evidence, therefore, for the general supposition that electrons and/or holes can move rapidly along the axis of column-stacked π-systems[5,6]. The decrease in conductivity on going from the crystalline solid to the mesophase is attributed to a lower charge mobility. This is probably due to an increase in positional disorder of the porphyrin moieties[7] on melting of the hydrocarbon mantle.

We have found a similar decrease in the radiation-induced conductivity at the solid to mesophase transition of octa-alkoxy-substituted phthalocyanines. An isotropic liquid phase of these compounds is not, however, attainable within the temperature range of our equipment. They could not therefore be used to carry out the conclusive experiment of completely melting the material to see if long-range order was essential for conduction. The experiments on octa-n-alkoxy substituted phthalocyanines have, however, shown that the lifetime of the conductivity transient increases exponentially with the length of the alkyl tails[8]. This is taken to be strong evidence that the mobile charge carriers responsible are restricted to rapid diffusional motion along the phthalocyanine axis of a stack, with eventual charge recombination requiring stack-to-stack electron tunnelling through the hydrocarbon mantle.

The absolute value of $(\Delta\sigma/D)_0$ is related to the mobilities, μ, of the charge carrers, $\sum \mu = (\mu(-) + \mu(+))$, and the average energy required to produce one charge-carrier pair, E_p (in eV), by[3,4]

$$(\Delta\sigma/D)_0 = \sum \mu/E_p \qquad (1)$$

For organic compounds, the total initial yield of electron–hole pairs corresponds to a value of E_p of ~25 eV for high-energy radiation[9-11]. Only a fraction of the initial electrons and holes will escape rapid (subnanosecond) geminate recombination[8,9] and diffuse to separate columns, thus being observed in the present experiments. Using a value of $E_p = 25$ eV together with the experimentally determined value of $(\Delta\sigma/D)_0$ will therefore yield a lower limit to the charge-carrier mobilities. For the solid phase of ZnP at room temperature, assuming electrons and holes to have almost equal mobilities[12], this gives $\mu > 2.6 \times 10^{-6}$ m^2 V^{-1} s^{-1} and for the mesophase, it gives $\mu > 0.6 \times 10^{-6}$ m^2 V^{-1} s^{-1}.

This order of magnitude of the mobility indicates small polaron motion[13] corresponding to the hopping of a more or less localized charge between neighbouring sites with an average jump time between sites of τ_j. The mobility measured in the present, randomly orientated columnar materials is related to τ_j by

$$\tau_j = ed_j^2/6k_BT\mu \qquad (2)$$

where d_j is the distance moved along the columnar axis per jump (4.9 Å for the present systems). The minimum values of the carrier mobilities given above correspond therefore to

maximum jump times of 0.6 and 2 ps for solid ZnP at room temperature and the mesophase at 100 °C, respectively.

Our results confirm that the transport of charge can occur very rapidly within an organized self-assembly of porphyrin moieties even in a relatively flexible, liquid crystalline phase. Such peripherally hydrocarbon substituted compounds may therefore be considered to provide model systems which crudely mimic the channelling of energy and charge found in the highly varied antenna chlorophyll arrays of photosynthetic membranes. □

1. Gregg, B. A., Fox, M. A. & Bard, A. J. *J. Am. chem. Soc.*, **111**, 3024–3029 (1989).
2. Weber, P., Guillon, D. & Skoulios, A. *Liq. Cryst.* **9**, 369–382 (1991).
3. Warman, J. M. & de Haas, M. P. in *Pulse Radiolysis*, Ch. 6. (ed. Tabata, Y.) 101–133 (CRC, Boca Raton, 1991).
4. Warman, J. M. & de Haas, M. P. *Radiat. Phys. Chem.* **34**, 581–586 (1989).
5. Eley, D. D. *Molec. Cryst. Liq. Cryst.* **171**, 1–21 (1989).
6. Simon, J. & André, J-J. *Molecular Semiconductors* (Springer, Berlin, 1985).
7. Pietro, W. J., Marks, T. J. & Ratner, M. A. *J. Am. chem. Soc.* **107**, 5387–5391 (1985).
8. Warman, J. M., de Haas, M. P., van der Pol, J. F. & Drenth, W. *Chem. Phys. Lett.* **164**, 581–586 (1989).
9. Warman, J. M. in *The Study of Fast Processes and Transient Species by Electron Pulse Radiolysis* (eds Baxendale, J. H. & Busi, F.) 433–533 (Reidel, Dordrecht, 1982).
10. Schmidt, W. F. & Allen, A. O. *J. Phys. Chem.* **72**, 3730–3736 (1968).
11. Shinsaka, K. & Freeman, G. R. *Can. J. chem.* **52**, 3495–3506 (1974).
12. Cox, C. A. & Knight, P. C. *J. Phys. C.* **7**, 146–156 (1974).
13. Mott, N. F. *Conduction in Non-Crystalline Materials*, Ch. 6 (Clarendon, Oxford, 1987).

A low-cost, high-efficiency solar cell based on dye-sensitized colloidal TiO$_2$ films

Brian O'Regan* & Michael Grätzel†

Institute of Physical Chemistry, Swiss Federal Institute of Technology, CH-1015 Lausanne, Switzerland

THE large-scale use of photovoltaic devices for electricity generation is prohibitively expensive at present: generation from existing commercial devices costs about ten times more than conventional methods[1]. Here we describe a photovoltaic cell, created from low- to medium-purity materials through low-cost processes, which exhibits a commercially realistic energy-conversion efficiency. The device is based on a 10-μm-thick, optically transparent film of titanium dioxide particles a few nanometres in size, coated with a monolayer of a charge-transfer dye to sensitize the film for light harvesting. Because of the high surface area of the semiconductor film and the ideal spectral characteristics of the dye, the device harvests a high proportion of the incident solar energy flux (46%) and shows exceptionally high efficiencies for the conversion of incident photons to electrical current (more than 80%). The overall light-to-electric energy conversion yield is 7.1–7.9% in simulated solar light and 12% in diffuse daylight. The large current densities (greater than 12 mA cm^{-2}) and exceptional stability (sustaining at least five million turnovers without decomposition), as well as the low cost, make practical applications feasible.

Solar energy conversion by photoelectrochemical cells has been intensively investigated[2-11]. Dye-sensitized cells differ from the conventional semiconductor devices in that they separate the function of light absorption from charge carrier transport. In the case of n-type materials, such as TiO$_2$, current is generated when a photon absorbed by a dye molecule gives rise to electron injection into the conduction band of the semiconductor, Fig. 1. To complete the circuit, the dye must be regenerated by

* Present address: Department of Chemistry, University of Washington, Seattle, Washington 98195, USA.
† To whom correspondence should be addressed.

electron transfer from a redox species in solution which is then reduced at the counter electrode. The monochromatic current yield

$$\eta_i(\lambda) = \text{LHE}(\lambda) \times \phi_{inj} \times \eta_e \qquad (1)$$

where LHE (light harvesting efficiency) is the fraction of the incident photons that are absorbed by the dye, ϕ_{inj} is the quantum yield for charge injection and η_e is the efficiency of collecting the injected charge at the back contact, expresses the ratio of measured electric current to the incident photon flux at a given wavelength. The photovoltage ΔV in Fig. 1, generated by the cell, corresponds to the difference between the Fermi level in the semiconductor under illumination and the Nernst potential of the redox couple in the electrolyte.

Although attempts to use dye-sensitized photoelectrochemical cells in energy conversion have been made before, the efficiency of such devices has been extremely low and practical applications have seemed remote. One problem is that of poor light harvesting. On a smooth surface, a monomolecular layer of sensitizer absorbs less than 1% of incident monochromatic light. Attempts to harvest more light by using multilayers of dye have in general been unsuccessful. The remaining option is to increase the roughness of the semiconductor surface so that a larger number of dye molecules can be adsorbed directly to the surface and can simultaneously be in direct contact with the redox electrolyte. Matsumura et al.[12] and Alonso et al.[13] have used sintered ZnO electrodes to increase the efficiency of sensitization by rose bengal and related dyes. Willig, Parkinson and colleagues[14] have reported high quantum yields for the dye sensitization of SnS$_2$. But the conversion yields from solar light to electricity remained well below 1% for these systems. In addition, the instability of the dyes employed presented a severe practical drawback. By using semiconductor films consisting of nanometer-sized TiO$_2$ particles, together with newly developed charge-transfer dyes, we have improved the efficiency and stability of the solar cell.

High-surface-area TiO$_2$ films were deposited on a conducting glass sheet from colloidal solutions. A transmission electron micrograph of the colloid is shown in Fig. 2. Electronic contact between the particles was produced by brief sintering at 450 °C. The size of the particles and pores making up the film is controlled by the size of the particles in the colloidal solution. The internal surface area of the film is determined by the size of the particles and the thickness of the film. These parameters were optimized to obtain efficient light harvesting while maintaining a pore size large enough to allow the redox electrolyte to diffuse

easily. Films of 10 μm thickness consisting of particles with an average size of 15 nm gave linear photocurrent response up to full sunlight and were used throughout. A cubic close packing of 15-nm-sized spheres to a 10-μm-thick layer is expected to produce a 2,000-fold increase in surface area.

Absorption spectra obtained for such nanostructured TiO$_2$ films are shown in Fig. 3. Bare films are transparent and colourless, displaying the fundamental absorption edge of anatase (band gap 3.2 eV) in the ultraviolet region. Deposition of a monolayer of the trimeric ruthenium complex[15,16], RuL$_2$(μ-(CN)Ru(CN)L$'_2$)$_2$, 1, where L is 2,2' bipyridine-4,4'-dicarboxylic acid and L' is 2,2'-bipyridine, results in deep brownish-red coloration of the film. The absorption onset is shifted to 750 nm, the light harvesting efficiency reading almost 100% in the whole visible region below 550 nm. Integration of the spectral overlap between a solar emission of AM1.5 and this absorption band shows that 46% of the incident solar energy flux is harvested by the dye coated film (AM = 1/sin α where α is the angle of incidence of the solar rays at the Earth's surface).

The optical density of the film at 478 nm corrected for the absorption by the conducting glass support was 2.45. Dividing by the extinction coefficient[16] of 1 ($e_{478} = 1.88 \times 10^7$ cm^2 mol^{-1}) yields the dye surface concentration, $\Gamma = 1.3 \times 10^{-7}$ mol cm^{-2}. As each dye molecule occupies an area[16] of 1 nm^2, the inner surface of the film is 780 cm^2 for each 1 cm^2 of geometric surface. Thus, the roughness factor is 780, which is smaller than the predicted value of 2,000. The difference is attributed to necking between TiO$_2$ particles. In addition, the large size of 1 prevents its access to very small pores, reducing the apparent surface area.

The photocurrent action spectrum obtained with the dye-coated TiO$_2$ film is also shown in Fig. 3. It closely matches the absorption spectrum, indicating that the current is due to electron injection from 1 into the conduction band of TiO$_2$. The photocurrent yield measured at 520 nm was found to depend

FIG. 2 Transmission electron micrograph of TiO$_2$ particles used in thin film production. The scale bar represents 10 nm. Particles were prepared by hydrolysis of titanium tetraisopropoxide[18,19] followed by autoclaving for 12 h at 200 °C. To form films the sol was concentrated by evaporation of water in vacuum at 25 °C until a viscous liquid was obtained. Carbowax M-20,000 (40% by weight of TiO$_2$) was added and the viscous dispersion (TiO$_2$ content 20% by weight) was spread on the conducting glass support (Asahi glass, fluorine-doped SnO$_2$ overlayer, transmission 85% in the visible, sheet resistance 80/square) to give a membrane of 10 μm thickness. This was heated under air for 30 min at 450 °C. High-resolution scanning electron microscopy revealed TiO$_2$ films to be composed of a three-dimensional network of interconnected nanoscale particles[19]. Transmission electron micrographs of TiO$_2$ particles were taken before heat treatment; the annealing of 450 °C did not induce significant changes in particle size. Before dye coating, a few monolayers of TiO$_2$ were electrodeposited onto the colloidal TiO$_2$ film from a Ti(III) solution. Detailed description of this procedure will be published elsewhere (L. Kaven, B.O'R., A. Kay and M.G., manuscript in preparation).
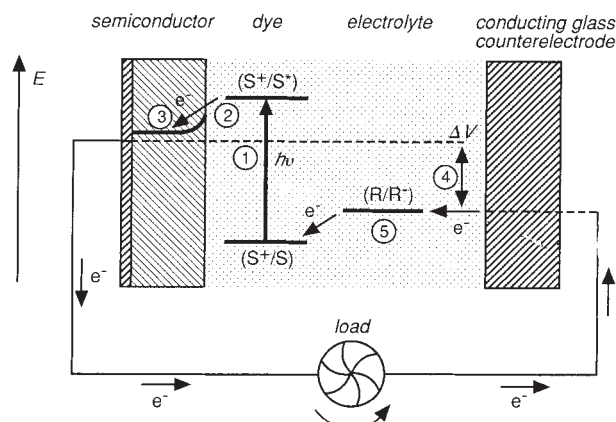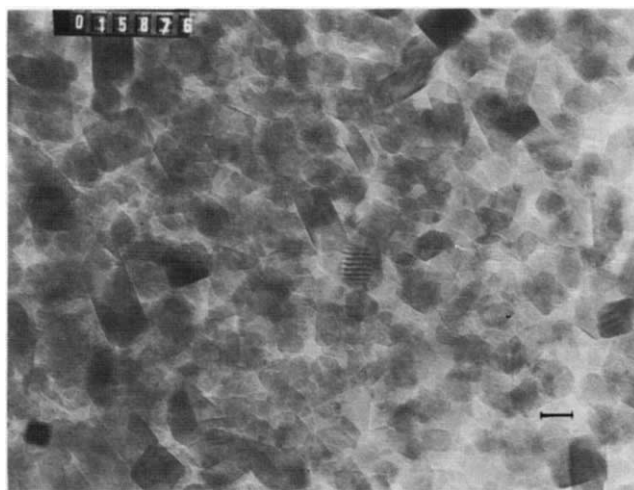

FIG. 1 Schematic representation of the principle of the dye-sensitized photovoltaic cell to indicate the electron energy level in the different phases. The cell voltage observed under illumination corresponds to the difference, ΔV, between the quasi-Fermi level of TiO$_2$ under illumination and the electrochemical potential of the electrolyte. The latter is equal to the Nernst potential of the redox couple (R/R$^-$) used to mediate charge transfer between the electrodes. S, sensitizer; S*, electronically excited sensitizer; S$^+$, oxidized sensitizer.

on the counter ion of the iodide/triiodide redox electrolyte, increasing from 68% for tetrapropylammonium to 84% for Li^+. After correction for the light absorption by the conducting glass, the yields are 80% and 97%, respectively. This shows that the nanostructured TiO_2 films used in conjunction with suitable charge transfer dyes can achieve quantitative conversion of visible light photons into electric current.

Figure 4 shows the current–voltage characteristics obtained with the thin layer cell under illumination by simulated AM1.5 solar light. The conversion efficiencies for one tenth and full sunlight are 7.9% and 7.12%, and the fill factors (maximum output power of cell $\div$ [short circuit current $\times$ open circuit voltage]) are 0.76 and 0.685, respectively. Similar yields were obtained under direct sunlight (measurements performed in June early in the afternoon on the roof of the institute). Under diffuse daylight the efficiency increased to 12%, indicating that under such conditions the cell performance is better than that of conventional silicon devices. This is because the spectral distribution of diffuse daylight overlaps more favourably with the absorption spectrum of the dye-coated TiO_2 film than direct sunlight. The fill factor of the cell remains above 0.7 even at very low light intensity (<5 W m^{-2}). Conventional photovoltaic cells have a much smaller fill factor (<0.5) under these conditions. This indicates that loss mechanisms such as recombination, normally encountered in semiconductor photoconversion, have been minimized. This result might appear surprising in view of the disordered structure of our film giving rise to defects. But the role of the semiconductor in a dye-sensitized device is merely to conduct the injected majority charge carriers. There are no minority carriers involved in the photoconversion process. Therefore, surface and bulk recombination losses due to lattice defects, encountered in conventional photovoltaic cells, are not observed in such a device.

The long-term stability of cell performance was tested by illuminating the thin TiO_2 film loaded with 1 with visible ($\lambda > 400$ nm) light for 2 months. The change in the photocurrent was less than 10% over this period, during which a charge of $62,000$ C cm^{-2} was passed through the device, corresponding to a turnover number of 5×10^6 for the sensitizer. This implies that if any dye degradation had occurred its quantum yield (ϕ_{sec}) is less than 2×10^{-8}. As $\phi_{dec} = k_{dec}/\Sigma k$, the rate constant, k_{dec} s^{-1}, for excited-state decomposition (due to processes such as ligand loss) must be at least 10^{-8} times smaller than Σk, the sum of rate constants for all channels of dye deactivation. Because charge injection is the predominant channel, this sum is practi-
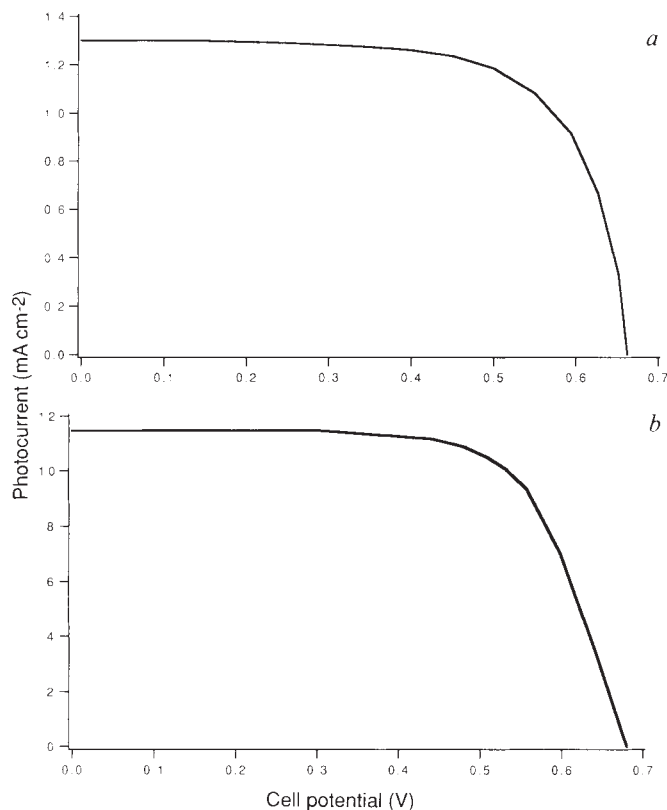

FIG. 4 Photocurrent–voltage characteristics of a cell, based on a colloidal TiO_2 film sensitized by 1; the film, supported on a conducting glass sheet, was used in a sandwich-type configuration. The size of the dye coated TiO_2 photoanode was 0.5 cm^2. The counterelectrode, consisting of conducting glass coated with a few monolayers of platinum, was placed directly on top of the working electrode. A thin layer of redox electrolyte is attracted into the intra-electrode space through capillary forces. The cell was exposed to simulated sunlight with AM1.5 spectral distribution. a, light intensity 83 W m^{-2}, electrolyte: 0.5 M tetrapropylammonium iodide +0.04 M iodine in a mixture of ethylene carbonate (80% by volume) with acetonitrile. Fill factor was 0.76; surface area 0.5 cm^2 (before multiplication by roughness factor). Conversion efficiency was 7.9%. b, light intensity 750 W m^{-2}, electrolyte: 0.5 M tetrapropylammonium iodide, 0.02 M KI $\times$ 0.04 M I_2 in the same solvent. Fill factor was 0.684; conversion was 7.12%.

cally equal to the rate constant for charge injection, which exceeds 10^{12} s^{-1} in the case of 1. Therefore, the upper limit for k_{dec} is 2×10^4 s^{-1}, which agrees with the known photophysics of this class of transition metal complexes[17]. The very fast electron injection observed with dyes such as 1, combined with high chemical stability, renders these compounds very attractive for practical development. □
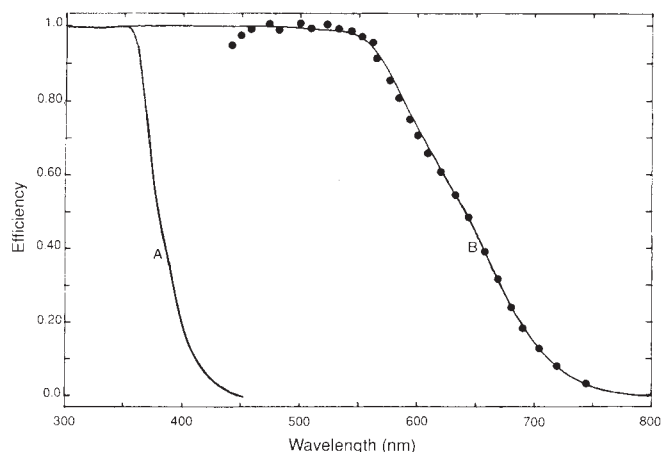

FIG. 3 Absorption and photocurrent action spectra of TiO_2 films supported on conducting glass. A, absorption efficiency of the bare TiO_2 film corrected for conducting glass background; B, absorption efficiency of the same film coated with a monolayer of 1; full circles, monochromatic current yield at short circuit as a function of excitation wavelength. Yield is corrected for 15% loss of incident photons through light absorption and scattering by the conducting glass support.

1. Bucher, K. & Fricke, J. Phys. Zeit 21, 237–244 (1980).
2. Honda, K. & Fujishima, A. Nature 238, 37–39 (1972).
3. Tufts, B. J. et al. Nature 326, 681–683 (1987).
4. Gerischer, H. Electrochim. Acta 35, 1677 (1990).
5. Licht, S., Hodes, G., Tenne, R. & Manassen, J. Nature 326, 863–864 (1987).
6. Heller, A. Acc. chem. Res. 14, 154–162 (1981).
7. Nozik, A. J. Phil. Trans. R. Soc. Lond. A295, 453–470 (1980).
8. Tributsch, H. & Bennet, J. C. J. electroanal. Chem. 81, 97 (1977).
9. Wrighton, M. S. Acc. chem. Res. 12, 303–310 (1979).
10. Bard, A. J. Science 207, 139 (1980).
11. Memming, R. Phil. Tech. Rev. 38, 160 (1979).
12. Matsumura, M., Nomura, Y. & Tsubomura, H. Bull. chem. Soc. Japan 50, 2533 (1977).
13. Alonso, N., Beley, V. M., Chartier, P. & Ern, V. Rev. Phys. Appl. 16, 5 (1981).
14. Willig, F., Eichberger, R., Sundaresan, N. S. & Parkinson, B. A. J. Am. chem. Soc. 112, 2702–2707 (1990).
15. Amadelli, R., Argazzi, R., Bignozzi, C. A. & Scandola, F. J. Am. chem. Soc. 112, 7099–7103 (1990).
16. Nazeeruddin, M. K., Liska, P., Moser, J., Vlachopoulos, N. & Grätzel, M. Helv. chim. Acta 73, 1788–1803 (1990).
17. Juris, A., Balzani, V., Barigletti, F., Campagna, S., Belzer, B. Coord. Chem. Rev. 84, 85 (1988).

18. Anderson, M. A., Gieselmann, M. J. & Xu, Q. *J. Membrane Sci.* **392**, 43 (1988).
19. O'Regan, B., Moser, J., Anderson, M. & Grätzel, M. *J. phys. Chem.* **94**, 8720–8726 (1990).

Super-spiral structures in an excitable medium

V. Perez-Muñuzuri*, R. Aliev, B. Vasiev, V. Perez-Villar* & V. I. Krinsky

Institute of Theoretical and Experimental Biophysics,
Academy of Sciences USSR, 142292 Pushchino, Moscow Region, USSR
* Departamento Fisica de la Materia Condensada, Facultad de Fisicas,
E-15706 University of Santiago de Compostela, Spain

ROTATING spiral waves have been observed in various excitable media, including heart muscle[1], retinae[2], cultures of the slime mould *Dyctiostelium discoideum*[3,4] and chemical oscillators such as the Belousov–Zhabotinsky (BZ) reaction[5–7]. Under certain conditions the spiral wave does not exhibit simple periodic rotation, but quasiperiodic[8] (or 'compound'[9]) rotation, in which the spiral's origin (the tip) meanders[10]. Recent calculations[11] have shown that highly meandering tip motion can impose superstructures on spiral waves. Here we reproduce these patterns experimentally, using the BZ reaction as the excitable medium. We induce high tip meander by applying pulses of electrical current locally at the tip[12]. Image processing of the patterns reveals a spiral wave of larger wavelength superimposed on the original wave, an effect that can be described in terms of a Doppler shift in the original spiral.

All our experiments were performed in a BZ reaction[13] in silica gel at room temperature (20 °C). A 0.9-mm-thick gel layer containing ferroin (0.008 M) was prepared in a Petri dish. During the experiments this layer was covered with a thick (6–8 mm) solution of the other BZ reaction components: 0.1 M $NaBrO_3$, 0.1 M $CH_2(COOH)_2$ and 0.5 M H_2SO_4.

The highly meandering tip motion needed for the production of superstructures was enhanced by using stepwise pulses of electric current[12] with a period of 11 min. In each period, the voltage (1.5 V, ~5 mA) was switched on for 4 min.

The electrical circuit used (analogous to that in ref. 12) included two electrodes immersed in the liquid layer. One of these was a circular electrode which ran around the border of the Petri dish, the other was needle-shaped (0.6 mm diameter). The needle was placed over the spiral tip (3 mm into the liquid layer). Two different types of electrodes, stainless steel and platinum, were used, with the same results.

The spiral wave dynamics were followed with a video recorder connected to a PC computer. To observe super-spiral waves, simple image processing was carried out: after acquiring two successive images (separated by 2 min), we subtracted the second from the first. This same procedure was used in the calculations of ref. 11. Contrast enhancement was then used to improve the quality of the printed pictures.

Spiral waves with many turns were created by the following procedure: at the beginning of the experiment, the sulphuric acid concentration was reduced (to ~0.2 M) to avoid the spontaneous appearance of wave sources. Spiral waves were produced in this medium by the breaking of a circular wave. To increase the frequency and the number of spiral turns, sulphuric acid was added until it reached its final concentration (0.5 M). This procedure made it possible to create a single vortex of ~14 turns, with period $T_s \approx 94$ s and wavelength $\lambda_s \approx 0.34$ cm (Fig. 1).

After the medium had become homogeneous, the spiral waves were perturbed by switching the current on and off. This resulted in the successive increasing and diminishing of the size of the core[12], so that the spiral tip described a 'flowerlet' pattern. The ratio of two frequencies associated with this motion was about six.

When this highly meandering tip motion occurs, the spiral shape becomes asymmetric. Some of the wavefronts that make up the spiral approach each other (see Fig. 2a). When the picture is processed by subtracting one image from another, a superstructure appears with the shape of a spiral wave (Fig. 2b). This super-spiral does not disappear with time, but rotates as the base spiral does; the tips of both spirals always coincide (Fig. 3). Note that the same results were observed numerically[11] (compare upper and lower parts of Fig. 2).

The period and wavelength of the super-spiral ($T_{ss} \approx 540$ s and $\lambda_{ss} \approx 2$ cm) proved to be six times as great as those of the base spiral. In contrast, the linear velocity was roughly equal for both spirals.

The super-spiral can be considered to be the result of the approach between fronts of the base spiral. In this case, the wave period detected at any point in the medium changes periodically with time. Figure 4a shows this effect, measured at a point near the centre of Fig. 2a.

The results presented in Fig. 4a can be interpreted by the Doppler effect. If we suppose that the waves of the spiral are emitted by a source rotating around a circle at constant velocity v_1 and period T_{ss}, then the period of waves at any point in the medium is given by the equation

$$T(t) = T_s \left\{ 1 + \frac{v_1}{v_0} \cos \left(2\pi \frac{t}{T_{ss}} + \phi \right) \right\} \qquad (1)$$
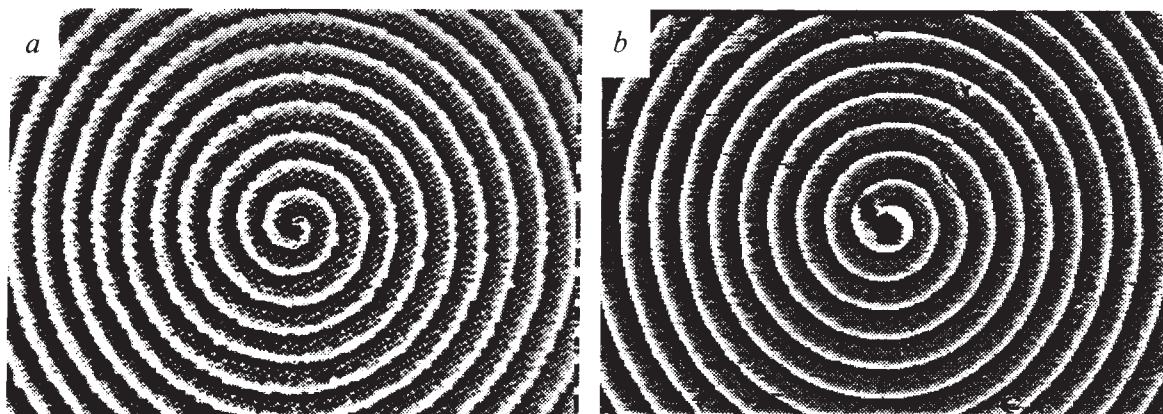

FIG. 1 Rigidly rotating spiral waves (a) for the phase-reaction/diffusion equation, $d\varphi/dt = R\{1 - \delta \sin(\varphi)\} + \alpha \nabla^2 \varphi + \beta |\nabla \varphi|^2$ (refs 11 and 15; and P. Hanusse and V.P.M., manuscript in preparation) and (b) in the BZ reaction.

The appearance and behaviour in the two cases are strikingly similar: constant wavelength, sharp fronts and rigid rotation around the centre. The black spot in the centre of b is the electrode shadow.